

# 1 Nonstationary time series prediction combined with slow feature analysis

2 G. Wang<sup>1</sup> and X. Chen<sup>1,2</sup>

3 1. Key Laboratory of Middle Atmosphere and Global Environment Observations, Institute of  
4 Atmospheric Physics, Chinese Academy of Sciences, Beijing 100029

5 2. Pingtan Meteorological Bureau of Fujian Province, Pingtan 350400

6  
7 *Correspondence to: G. Wang ([wgl@mail.iap.ac.cn](mailto:wgl@mail.iap.ac.cn))*  
8

9 **Abstract.** Almost all climate time series have some degree of nonstationarity due to  
10 external driving forces perturbing the observed system. Therefore, these external  
11 driving forces should be taken into account when constructing the climate dynamics.  
12 This paper presents a new technique of obtaining the driving forces of a time series  
13 from the Slow Feature Analysis (SFA) approach, then introducing them into a  
14 predictive model to predict non-stationary time series. The basic theory of the  
15 technique is to consider the driving forces as state variables and incorporate them into  
16 the predictive model. Experiments using a modified logistic time series and winter  
17 ozone data in Arosa, Switzerland, were conducted to test the model. The results  
18 showed improved prediction skills.

## 19 20 **1 Introduction**

21  
22 Many previous studies have concluded that the climate system is essentially  
23 non-stationary (Trenberth, 1990; Tsonis, 1996; Yang and Zhou, 2005; Boucharel et al.,  
24 2009). However, lacking of any general theory for predicting non-stationary processes  
25 has become one of the main barriers in the field of climate prediction. To unravel this  
26 issue, in recent years, increasing effort has been devoted to devising methods to  
27 analyze and predict nonstationary time series. (e.g. Hegger et al., 2000; Verdes et al.,  
28 2000, Wan et al, 2005; Wang and Yang, 2005; Yang et al., 2010) . The mostly used  
29 method in such studies was to remove or reduce the nonstationarity of the predicted  
30 system using some mathematical techniques, thereby improving the prediction skills.

31 The nonstationarity exists due to the fact that the driving forces that perturb the  
32 observed system change with time (Manuca and Savit, 1996). Consequently, the most

33 effective way to remove the nonstationarity may be to incorporate all the driving  
34 forces in the constructed dynamical system, and to consider them as the state variables  
35 of that system when establishing a prediction equation within a general circulation  
36 model (GCM). Based on this principle, lately a data-driven modeling path that  
37 compatible with GCM was proposed to predict several artificial non-stationary time  
38 series with known external forces. It has achieved success in improving predictions  
39 when driving forces were included in some ideal or climate systems, such as the  
40 Lorenz system, a logistic model, or global temperature over seasonal timescales  
41 including the North Atlantic Oscillation (NAO), the Pacific Decadal Oscillation  
42 (PDO), the El Niño/Southern Oscillation (ENSO), and the North Pacific Index (NPI)  
43 variability (Wang et. al., 2012, 2013). However, a disadvantage of this technique is  
44 that it can not differentiate the assumed driving forces from the predictive model.  
45 Therefore, in the present study we considered the extraction of driving forces from the  
46 time series itself and established a predictive model by incorporating the constructed  
47 driving forces. As a result, the extraction of driving forces became the focus of this  
48 study.

49 Wiscott (2003) developed a technique called Slow Feature Analysis (SFA) to  
50 extract driving forces from time series. This technique has been applied to  
51 nonstationary time series with some success (Wiskott, 2003; Berkes and Wiskott,  
52 2005; Gunturkun, 2010; Konen and Koch, 2011). In this paper, we used SFA to  
53 construct the driving forces from a testing time series, and then established a  
54 predictive model that incorporated the driving forces. The paper is organized as  
55 follows: A brief description of the predictive technique is presented in section 2. In  
56 section 3, results are reported from applying the approach to a modified logistic time  
57 series and the total ozone data of Arosa, Switzerland. A summary is provided in

58 section 4.

## 59 **2 Methodology**

60

61 SFA is a method that extracts slowly varying driving forces from a quickly varying  
62 non-stationary time series. In this section we provide a brief overview of SFA and its  
63 application on the extraction and construction of the driving forces from the time  
64 series. The details of SFA is presented in Wiscott (2003), but the basic steps of the  
65 technique are provided here for convenience and completeness. Let us assume that we  
66 have a single variable time series  $\{x(t)\}_{t=1,2,\dots,n}$  from a dynamical system:

67 1) Embed the above time series into an  $m$ -dimensional space (also named the  
68 length of the  $m$  window), a phase trajectory in the  $m$ -dimensional space denoted as

$$\begin{aligned} 69 \quad X(t) &= \{x(t), x(t-1), \dots, x(t-(m-1))\}_{t=1, \dots, N} \quad \text{or} \\ 70 \quad X(t) &= \{x_1(t), x_2(t), \dots, x_m(t)\}_{t=1, \dots, N} \end{aligned} \quad (1)$$

71 where  $N = n - m + 1$ .

72 2) Generate an expanded signal  $H(t)$  for a quadratic expansion, all monomials of  
73 degree one and two including mixed terms are used:

$$74 \quad H(t) = \{x_1(t), \dots, x_m(t), x_1^2(t), \dots, x_1(t)x_m(t), \dots, x_{m-1}^2(t), x_{m-1}(t)x_m(t), x_m^2(t)\}_{t=1, \dots, N}, \quad (2)$$

75 where  $H(t)$  is an  $k \times N$  matrix and  $k = m + m(m+1)/2$ .

76 To simplify (2) as

$$77 \quad H(t) = \{h_1(t), h_2(t), \dots, h_k(t)\}_{t=1, \dots, N}. \quad (3)$$

78 The general objective of SFA is to extract slowly varying features from the time  
79 series  $\{x(t)\}_{t=1,2,\dots,n}$ , in other words, to find a set of coefficients,  $W^* = (w_1^*, w_2^*, \dots, w_k^*)$ ,  
80 to make the output signal  $y^*(t) = W^* \bullet H(t)$  satisfy

$$(\dot{y}^* \dot{y}^{*T}) = \min_k \{(\dot{y}_k \dot{y}_k^T)\} \quad (4)$$

81

82 Here,  $\dot{y}_k$  is first-order derivative, calculated by  $\Delta y_k(t_i) = y_k(t_{i+1}) - y_k(t_i)$ .

83 3) Normalize the expanded signal  $H(t)$ , by an affine transformation to generate  $H'(t)$

84 with zero mean and unit covariance matrix:

$$H'(t) = \{h'_1(t), h'_2(t), \dots, h'_k(t)\}_{t=1, \dots, N} \quad (5)$$

85

86 Where  $\bar{h}'_j = 0$ ,  $h'_j h_j'^T = 1$ ,  $h'_j(t) = (h_j(t) - \bar{h}_j) / S$ , and  $S = \frac{1}{k} \sqrt{\sum_{j=1}^k (h_j(t) - \bar{h})^2}$

87 4) By means of the Schmidt algorithm, the function space (5) is orthogonalized as

$$\begin{aligned} z_1(t) &= h'_1(t) \\ z_j(t) &= h'_j(t) - \sum_{i=1}^{j-1} \frac{h'_{i+1}(t) \bullet z_i(t)}{\|z_i\|} z_i(t) \quad (j = 2, \dots, K) \end{aligned} \quad (6)$$

88

89 which is also denoted as  $Z(t) = \{z_1(t), z_2(t), \dots, z_k(t)\}_{t=1, \dots, N}$ . Here,  $z_i(t) \bullet z_j(t) = 0$

90 ( $i \neq j$ ) and it guarantees that every variable of the output is uncorrelated

91 5) Establish the covariance matrix of  $Z(t)$ , denoted as  $B = (\dot{Z}\dot{Z}^T)_{K \times K}$ . The  $k$

92 eigenvectors with smallest eigenvalues,  $\lambda_k$ , yield the normalized weight vectors

93 with  $\lambda_1 \leq \lambda_2 \leq \dots \leq \lambda_k$ , which can be easily found by principle component analysis.

94 The smallest eigenvalue,  $\lambda_1$ , corresponding to the eigenvector  $W_1$  can satisfy

95 equation (4), which represents the weight coefficient of the slowest varying

96 component. Here,  $W_1$  has a free scale factor (presented as  $r$ ), and then the slowest

97 varying variable, or the driving forcing, can be obtained by the following equation:

$$y_1(t) = r W_1 \bullet Z(t) + c, \quad (7)$$

98

99 Where  $c$  is a given constant and  $\{y_1(t)\}$  is the output signal of the slowest driving

100 force obtained by equation (7).

101

102 In this study, the SFA was tested on a logistic map

$$103 \quad s_{t+1} = \mu_t s_t (1 - s_t) \quad (8)$$

104 with a given driving force parameter

$$105 \quad \mu_t = 3.5 - 0.45 \cos(3\pi t / 1600) \exp(-t / 2500) \quad (9)$$

106 To test the ability to construct the driving force from this modified logistic map, we  
107 took a time series that consists of 5000 data points from this map. Applying the SFA  
108 algorithm on this time series with the embedded dimension chosen as 3, we  
109 constructed the driving force shown in Figure 1, in which the dotted line represents  
110 the true driving force given by (9) and the solid line the constructed driving force by  
111 the SFA approach. There is a good agreement between the constructed and the true  
112 driving forces with a correlation coefficient of 0.998. This suggests that SFA was able  
113 to extract the driving force from the observed time series in an unsupervised manner.

114 By far we have two time series, one is the original time series  $\{x(t)\}$ , the another is  
115 the slowest driving force  $\{y_1(t)\}$ . Next we demonstrate how to establish a predictive  
116 model that includes the driving force constructed by the SFA procedure described  
117 above. We present the basic principle to build the prediction model, for convenience,  
118 we assume a nonstationary process composes of two series,  $\{x(t)\}_{t=1,2,\dots,n}$  and  $\{y_1(t)\}$ ,  
119 with the former being the state variable time series and the latter as the constructed  
120 external driving force obtained through the SFA approach. The two time series were  
121 embedded in an  $m_1 + m_2$  dimensional phase space with a selected time lag  $\tau$ . The  
122 constructed phase trajectory using the embedding theorem of Takens (1981) is shown  
123 as:

$$124 \quad \vec{E}(t) = \{x(t), x(t - \tau), \dots, x(t - (m_1 - 1)\tau); y_1(t), y_1(t - \tau), \dots, y_1(t - (m_2 - 1)\tau)\}_{t=1,2,\dots,N} \quad (10)$$

125 Here,  $m_1$  and  $m_2$  are the given embedding dimensions for  $\{x(t)\}$  and  $\{y_1(t)\}$ ,

126 respectively, and  $N = \lceil (\max(m_1, m_2) - 1)\tau \rceil$  is the number of phase points on the  
 127 trajectory.

128 Based on this trajectory, a predictive model to predict the future state of the system  
 129 can be established as:

$$130 \quad x(t+p) = \hat{f}_p(\bar{x}(t); \bar{y}_1(t)) + \varepsilon(t) \quad (11)$$

131 Where  $p$  is the prediction time step (considered as 1 in the present study),  $\varepsilon(t)$  is the  
 132 fitting error, and  $\hat{f}$  is assumed to be a quadratic polynomial in this study. The Takens  
 133 embedding theorem is only appropriate for an autonomous dynamical system,  
 134 therefore we followed the method of Stark (1999) to embed the driving forces in the  
 135 same state space for a nonstationary system. The next task is to find the cost function

$$136 \quad \eta = \sum_{t=1}^N [f(x(t), y_1(t)) - x(t+1)]^2 \quad (12)$$

when it reaches its minimum value. For more  
 137 details, refer to the studies of Farmer and Sidorowich (1987) and Casdagli (1989).

### 138 **3 Experiments**

139 We applied the prediction technique described above to perform some prediction  
 140 experiments using several given non-stationary time series. The experiment presented  
 141 in Section 3.1 was performed with data from the modified logistic model given above.

#### 142 **3.1 Prediction experiments for ideal time series**

143 The prediction experiments were based on 5000 data points from the above verified  
 144 logistic map (8) with the assumed driving force (9). The first 4800 data points were  
 145 applied to establish the predictive model, and the remaining 200 data points were used  
 146 to test the prediction and estimate the correlation coefficient between the actual and  
 147 predicted values as a function of the prediction time step. The embedding dimension

148 of the verified logistic time series, namely  $m_1$ , took values from 2 to 3, and the  
149 embedding dimension of the driving force time series, namely  $m_2$ , was set to either 0  
150 (the driving force was not taken into account, and is referred to as the ‘stationary  
151 model’ hereinafter) or 1 (the driving force extracted from the verified logistic map by  
152 SFA was taken into account, and is referred to as the ‘forcing model’ hereinafter). The  
153 time lag  $\tau$  was always set to be 1. Figure 2 shows the prediction skill with and without  
154 the influence of the driving force, which was constructed by the SFA approach. The  
155 forcing model excelled over the stationary model. In particular, at the fourth  
156 prediction step, the correlation coefficients were below 0.2 in the stationary model  
157 compared to above 0.6 in the forcing model. The average correlation across the  
158 prediction time steps was improved, indicating that introducing the driving force  
159 extracted through the SFA approach into the prediction model can yield a significant  
160 improvement in accuracy.

161

### 162 **3.2 Prediction experiment for total ozone**

163 Many studies have sought to explain the variables involved in ozone dynamics, such  
164 as the Quasi-Biennial Oscillation (QBO), the 11-year solar cycle, volcanic eruptions,  
165 the El Niño Southern Oscillation (ENSO), North Atlantic Oscillation (NAO) (e.g.,  
166 Brasseur and Granier, 1992; Hood, 1997; Schmidt et al., 2010; Rieder et al., 2010). In  
167 this paper we focused on prediction experiments with total ozone data. The total  
168 ozone data were from Arosa, Switzerland, and were the world’s longest total ozone  
169 record. Homogenized total ozone data from 1927 to 2007 were obtained from the

170 World Ozone and Ultraviolet Radiation Data Centre (WOUDC;  
171 <http://www.woudc.org>).

172 By using the SFA technique on Arosa's daily total ozone data in winter (from  
173 January to March) for the period 1927 to 2007, we obtained the first output of the  
174 driving force  $\{y_1\}$  when the embedding dimension was chosen as 3,5,7,9,11,  
175 respectively (shown in Figure 3). Note that the result did not change significantly with  
176 different embedding dimension values.

177 We established a prediction model for winter ozone data by incorporating the  
178 driving force constructed by SFA. The prediction was based on 7305 data points. Out  
179 of the 7305 data points, the first 7125 data points were used to build the predictive  
180 model, and the remaining 180 data points were used to test the prediction using  
181 root-mean-square error (RMSE) and the correlation coefficient between observed and  
182 predicted values. The time lag  $\tau$  was taken to be 1, the embedding dimension of the  
183 total ozone data  $m_1$  took values from 3 to 5, and the embedding dimension of the  
184 driving force time series  $m_2$  was set to either 0 for the stationary model or 3 to 5 for  
185 the forcing model.

186 The experimental results for this case are listed in Table 1, also shown in Figure 4  
187 and Figure 5. From Table 1, it can be seen that all RMSE values given by the forcing  
188 model were much lower than those by the stationary model. Figure 4 presents the  
189 correlation coefficients between the observed and predicted values. The forcing model  
190 outperformed the stationary model, especially at the first two steps. At the first  
191 prediction step, the correlation coefficients reached 0.61 for the stationary model but  
192 0.91 for the forcing model. At the 8th prediction step, the correlation coefficients  
193 reduced to 0.39 for the stationary model, but still maintained at 0.45 for the forcing  
194 model. At the 12th prediction step, the correlation coefficients were 0.22 and 0.33 for

195 the stationary model, and the forcing model respectively. This has clearly shown that,  
196 when the constructed driving force is introduced, the accuracy of prediction is  
197 dramatically improved. The average correlation over the prediction time steps is  
198 improved by 50% when the driving force extracted through SFA technique is included.  
199 Figure 5 illustrates the error between the prediction and observation. The prediction  
200 errors for every time step is lower for the forcing model than the stationary model. All  
201 these results indicate that the inclusion of the driving force constructed by the SFA  
202 approach into the prediction model largely improve the predictive skill of winter total  
203 ozone in Arosa. Some sensitivity analysis with different training/verifying lengths do  
204 not alter this conclusion.

#### 205 **4 Discussion**

206  
207 In this study, we first constructed the driving forces of a time series based on the SFA  
208 approach, and then the driving forces were introduced into a predictive model. By  
209 doing so, we extend the study by Wang et. al. (2012, 2013) and present a novel  
210 technique to predict non-stationary time series. Unlike the former works by Wang et.  
211 al. (2012, 2013) with assumed driving forces, in this study the driving force was  
212 extracted from original time series. The experimental results obtained from a modified  
213 logistic time series and winter ozone data in Arosa confirmed the effectiveness of the  
214 model.

215 The driving force construction technique based on SFA represents a progress for  
216 climate causal relations. Such an approach may provide a compatible and direct  
217 window for studying causality using external driving forces. We constructed the  
218 driving forces with SFA and then combined these driving forces to establish the  
219 predictive model. Although we found this approach was able to effectively improve

220 the predictive ability, the constructed driving force time series still lacks of physical  
221 explanation. In order to understand the real background of these, one has to further  
222 explore the physical processes behind it. One recommended method, provided by  
223 Verde s (2005), suggests using a measure called ‘transfer entropy’ to analyze the  
224 causality; another recommended method is named ‘convergent cross mapping’  
225 provided by Sugihara et. al. (2012), which measures causality in nonlinear dynamic  
226 systems. Work in this area is in progress and will be reported in future publications.

227

228 **Acknowledgments.** This research was supported by the National Natural Science  
229 Foundation of China under Grant 41275087. The authors are grateful to the editor and  
230 three anonymous referees for useful comments during the discussion phase in NPGD.

231

## 232 **References**

233

- 234 Berkes, P., Wiskott, L.: Slow feature analysis yields a rich repertoire of complex cell  
235 properties, *Journal of Vision*, 5, 579-602, 2005.
- 236 Boucharel, J., Dewitte, B., Garel, B., Penhoat, Y.: ENSO’s non-stationary and  
237 non-Gaussian character: the role of climate shifts, *Nonlin. Processes Geophys.*,  
238 16, 453–473, 2009.
- 239 Brasseur, G., Granier, C.: Mount Pinatubo aerosols, chlorofluorocarbons and ozone  
240 depletion, *Science*, 257, 1239–1242, 1992.
- 241 Casdagli, M.: Nonlinear prediction of chaotic time series, *Phys. D.*, 35, 335–356,  
242 1989.
- 243 Farmer, J. D., Sidorowich, J.: Predicting chaotic time series, *Phys. Rev. E.*, 59,  
244 845–848, 1989.
- 245 Gunturkun, U.: Sequential reconstruction of driving-forces from nonlinear  
246 nonstationary dynamics, *Phys. D.*, 239, 1095-1107, 2010.
- 247 Hegger, R., Kantz, H., Matassini, L., Schreiber, T.: Coping with non-stationarity by  
248 over-embedding, *Phys. Rev. E.*, 84, 4092–4101, 2000.

249 Hood, L.: The solar cycle variation of total ozone: Dynamical forcing in the lower  
250 stratosphere, *J Geophys Res.*, 102, 1355-1370, 1997.

251 Konen, W., Koch, P.: The slowness principle: SFA can detect different slow  
252 components in non-stationary time series, *Int. J. Innovative Computing and*  
253 *Applications*, 3, 3-10, 2011.

254 Manuca, R., Savit, R.: Stationarity and nonstationarity in time series analysis, *Phys.*  
255 *D.*, 99, 134–161, 1996.

256 Rieder, H. E., Staehelin, J., Maeder, J. A., Peter, T., Ribatet, M., Davison, A. C.,  
257 Stubi, R., Weihs, P., Holawe, F.,: Extreme events in total ozone over Arosa – Part  
258 2: Fingerprints of atmospheric dynamics and chemistry and effects on mean  
259 values and long-term changes, *Atmos Chem Phys.*, 10,10033--10045, 2010.

260 Schmidt, H., Brasseur, G Giorgetta, M., : Solar cycle signal in a general circulation  
261 and chemistry model with internally generated quasi - biennial oscillation, *J*  
262 *Geophys Res.*, 115,D00I14, doi:10.1029/2009JD012542, 2010.

263 Stark. J.: Delay embeddings for forced systems: deterministic forcing, *Journal of*  
264 *Nonlinear Science*, 9, 255–332,1999.

265 Sugihara, G, May,R., Ye, H., Hsieh, C., Deyle, E., Fogarty, M., Munch, S.: Detecting  
266 causality in complex ecosystems, *Science*, 338, 496-500, Doi:10.1126/  
267 *Science.1227079*, 2012.

268 Takens, F.: Detecting Strange Attractors in Turbulence, *Dynamical Systems and*  
269 *Turbulence*, Heidelberg, Springer-Verlag, 366–381, 1981.

270 Trenberth, K. E.: Recent observed inter-decadal climate changes in the northern  
271 hemisphere, *Bull. Amer. Meteor. Soc.*, 7, 988–993, 1990.

272 Tsonis, A. A.: Widespread increases in low-frequency variability of precipitation over  
273 the past century, *Nature*, 382, 700–702, 1996.

274 Verdes, P. F., Parodi, M. A., Granitto, P. M., Navone, H. D., Piacentini, R. D.,  
275 Ceccatto, H. A. : Predictions of the maximum amplitude for solar cycle 23 and  
276 its subsequent behavior using nonlinear methods, *Sol. Phys.*, 191(2), 419 – 425,  
277 2000.

278 Verdes, P. F.: Assessing causality from multivariate time series, *Phys. Rev. E.*, 72,  
279 026222, 2005.

280 Wan, S., Feng, G, Zhou, G, Wan, B., Qin, M., Xu, X. : Extracting useful information  
281 from the observations for the prediction based on EMD method, *Acta*  
282 *Meteorologica Sinica*, 63, 516–525, 2005.

283 Wang, G., Yang, P.: A compound reconstructed prediction model for nonstationary  
 284 climate process, *Inter. J. Climatol*, 25,1265–1277, 2005.

285 Wang, G., Yang, P., Zhou, X., Swanson, K., Tsonis, A.: Directional influences on  
 286 global temperature prediction, *Geophys. Res. Lett.*, 39, L13704, doi:10.1029/  
 287 2012GL052149, 2012.

288 Wang, G., Yang, P., Zhou, X.: Nonstationary time series prediction by incorporating  
 289 external forces, *Adv. Atmos. Sci.*, 30, 1601-1607, 2013.

290 Wiskott, L.: Estimating driving forces of nonstationary time series with slow feature  
 291 analysis, arXiv.org e-Print archive, <http://arxiv.org/abs/cond-mat/0312317/>,  
 292 2003.

293 Yang, P., Zhou, X.: On nonstationary behaviors and prediction theory of climate  
 294 systems, *Acta Meteorologica Sinica*, 63, 556-570, 2005

295 Yang, P., Wang, G., Bian, J., Zhou, X.: The prediction of non-stationary climate series  
 296 based on empirical mode decomposition, *Adv. Atmos. Sci.*, 27(4), 845–854, doi:  
 297 10.1007/s00376-009-9128-x, 2010.

298  
 299  
 300  
 301

302 Table 1 RMSE comparison of the prediction experiments (unit: Dobson units)

303

|                  | <i>1</i> | <i>2</i> | <i>3</i> | <i>4</i> | <i>5</i> | <i>6</i> | <i>7</i> | <i>8</i> | <i>9</i> | <i>10</i> |
|------------------|----------|----------|----------|----------|----------|----------|----------|----------|----------|-----------|
| Stationary model | 0.80     | 0.88     | 0.90     | 0.94     | 0.96     | 0.99     | 1.03     | 1.02     | 1.04     | 1.05      |
| Forcing model    | 0.62     | 0.55     | 0.62     | 0.74     | 0.87     | 0.93     | 0.97     | 0.98     | 1.01     | 1.01      |

304  
 305  
 306  
 307  
 308  
 309  
 310

311 **Figure Captions**

312 Figure 1 The true and constructed driving force.

313 Figure 2 The comparison of prediction skills between models combined with or  
314 without driving force.

315 Figure 3 The slowest driving force with different embedding dimension for total  
316 ozone data.

317 Figure 4 The comparison of prediction skills between models combined with or  
318 without driving force.

319 Figure 5 Errors (Dobson Units) at prediction steps with or without forcing input.

320

321

322

323

324

325

326

327

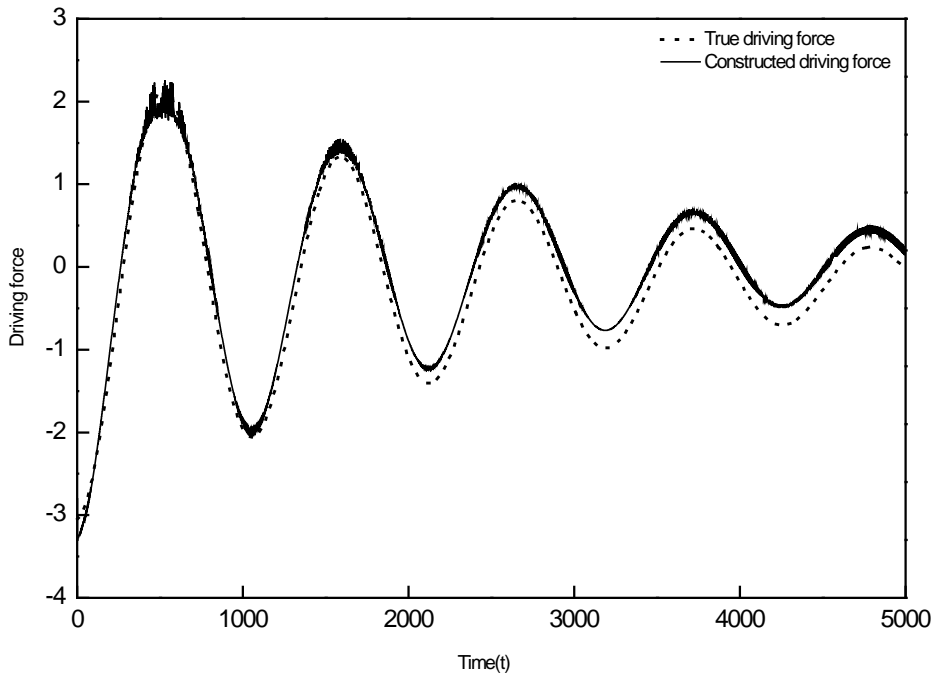
328

329

330

331

332



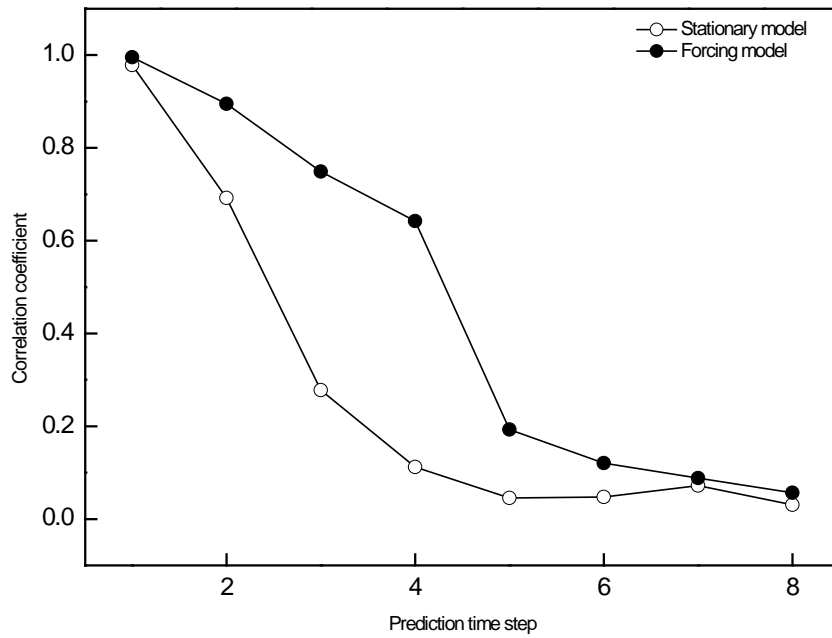
333

334

Figure 1 The true and constructed driving force.

335

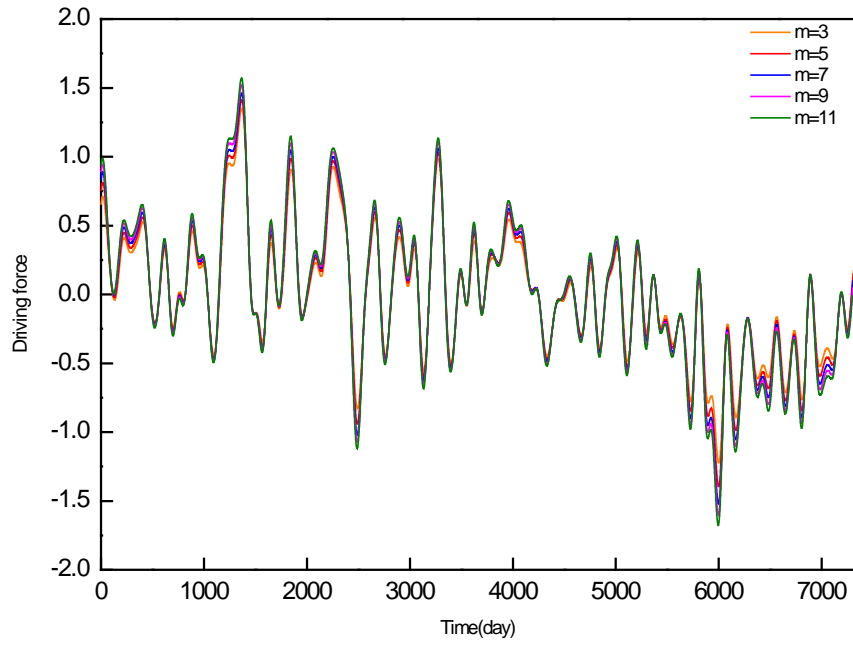
336



337

338 Figure 2 The comparison of prediction skills between models combined with or without driving  
339 force.

340

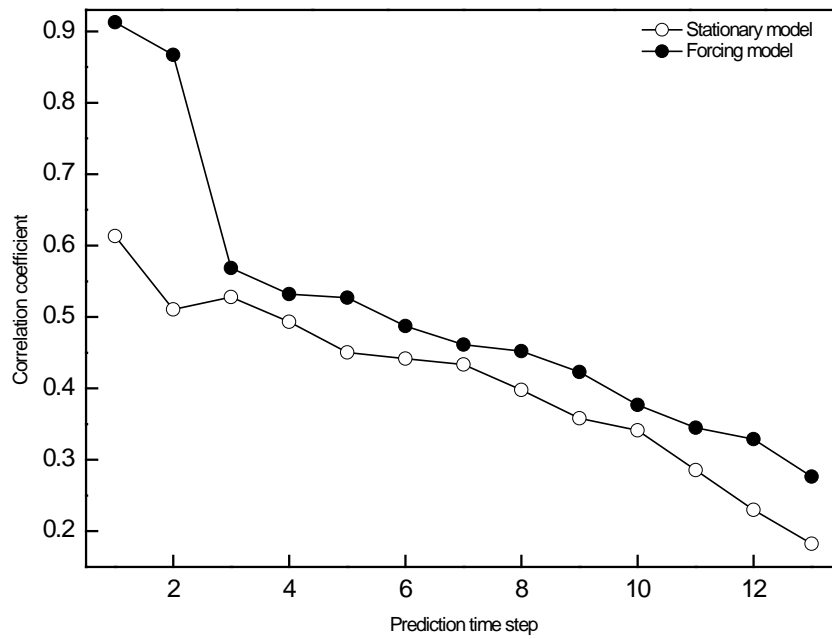


341

342 Figure 3 The slowest driving force with different embedding dimension for total ozone data.

343

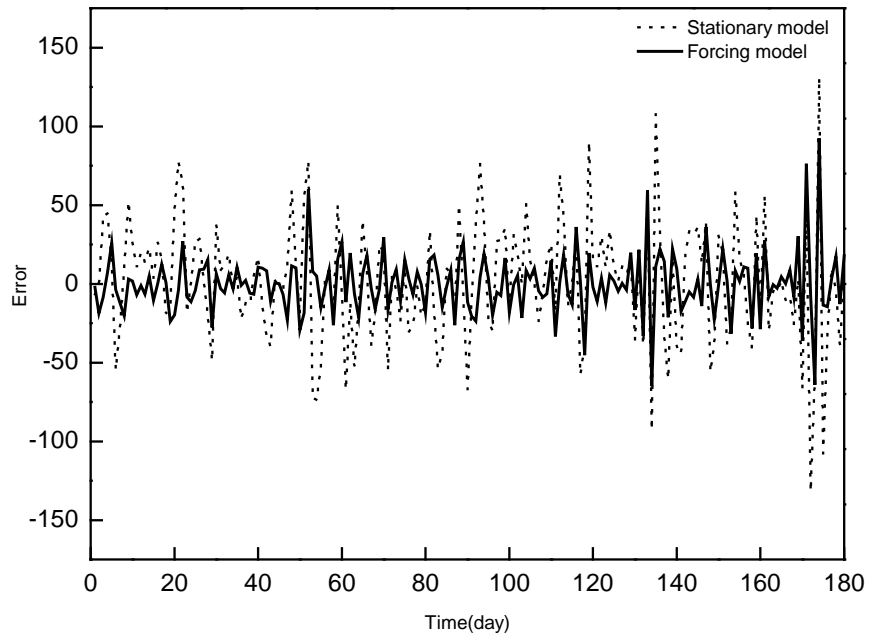
344



345

346 Figure 4 The comparison of prediction skills between models combined with or without driving force.

347



348

349 Figure 5 Errors (Dobson Units) at prediction steps with or without forcing input.

350